EMPIRICAL MODE DECOMPOSITION ANALYSIS OF CLIMATE CHANGES WITH SPECIAL REFERENCE TO RAINFALL DATA

MD. KHADEMUL ISLAM MOLLA, M. SAYEDUR RAHMAN,
AKIMASA SUMI, AND PABITRA BANIK

Received 27 July 2005; Accepted 6 November 2005

We have used empirical mode decomposition (EMD) method, which is especially well fitted for analyzing time-series data representing nonstationary and nonlinear processes. This method could decompose any time-varying data into a finite set of functions called "intrinsic mode functions" (IMFs). The EMD analysis successively extracts the IMFs with the highest local temporal frequencies in a recursive way. The extracted IMFs represent a set of successive low-pass spatial filters based entirely on the properties exhibited by the data. The IMFs are mutually orthogonal and more effective in isolating physical processes of various time scales. The results showed that most of the IMFs have normal distribution. Therefore, the energy density distribution of IMF samples satisfies χ^2-distribution which is statistically significant. This study suggested that the recent global warming along with decadal climate variability contributes not only to the more extreme warm events, but also to more frequent, long lasting drought and flood.

1. Introduction

Several linear statistical models have been applied to climatic data (Rajagopalan et al. [19, 20], Harrison and Larkin [11], and Wunsch [27]), but the results are not conclusive due to the high sensitivity of model results to model parameters (Rajagopalan et al. [19, 20] and Harrison and Larkin [11]), especially when stochastic processes are taken into account (Wunsch [27]).

A new nonlinear technique, empirical mode decomposition (EMD), has recently been pioneered by Huang et al. [13] for adaptively representing nonstationary time-series data. Although it proved remarkably effective (Huang et al. [13] and Wu et al. [26]), the technique is faced with the difficulty of being essentially defined by an algorithm and therefore

Hindawi Publishing Corporation
Discrete Dynamics in Nature and Society
Volume 2006, Article ID 45348, Pages 1–17
DOI 10.1155/DDNS/2006/45348

does not admit an analytical formulation which would allow for a theoretical analysis and performance evaluation.

Spatial rainfall data contain information of a broad range of spatial scales (Pegram and Clothier [18]; Harries et al. [10] and Turner et al. [23]). The technique employed is a two-dimensional generalization of the one-dimensional EMD technique introduced by Huang et al. [13]. In a single dimension, EMD analysis produces a set of intrinsic mode functions (IMFs) that are very nearly orthogonal. The key contribution of Sinclair and Pegram [22] paper is to introduce the concept of 2D EMD to the hydrometeorological literature as a tool for the analysis of spatio-temporal rainfall data. The EMD algorithm copes with stationary by ignoring the concept, embracing nonstationary as a practical reality. Although EMD is relatively new data analysis technique, its power and simplicity have encouraged its application in different fields.

The El Nino and the southern oscillation phenomenon (ENSO) is the primary driver of interannual climate variability and has a large economic and social impact over the universe (Glantz et al. [8]). Fedorov and Philander [6] demonstrated that mean fluctuations of decadal timescale do contribute significantly to the later unusual ENSO events and suggested that global warming cannot be ruled out as a suspect (Wu et al. 2002).

Chiew et al. [3] examine the one-dimensional EMD of several annual stream flow time series to search for significant trends in the data, using bootstrapping to test the statistical significance of identified trends. The technique has been extensively used in ocean wave data analysis (Huang et al. [12]; Hwang et al. [15]) as well as in the analysis of polar ice cover (Gloersen and Huang, [9]). EMD has also been applied in the analysis of seismological data by Zhang et al. [28] and also has been used to diagnose heart beat rate fluctuations (Balocchi et al. [1]). Also some used in signal image processing (Flandrin et al. [7]).

Global climate change is one of the most controversial issues to the scientific community. Some of the most important data associated with global climate change is rainfall. Global warming is one of the most serious global environmental issues facing mankind. Climate is a fundamental component of the Earth's natural system. Effect of global warming is already visible. The global mean temperature has increased by 0.6 °C over the last century and many organisms and ecosystems have experienced changes. There is a perception that extreme natural disasters such as floods, droughts, and heat waves have become more frequent. This change in climate plays an important role in the Earth's sustainability.

2. Data and methodology

2.1. Rainfall data. All the weather parameters were measured with instruments specified by India Meteorological Department, Government of India. Daily rainfall data were collected from the Agricultural Experimental Farm, Indian Statistical Institute, Giridih, Jharkhand for the years 1989 to 2004. Rainfall was measured with IMD specified manual and automatic rain gauges. Onset of monsoon during different years was identified as the week which received more than 20 mm of rain in 1 or 2 consecutive days, provided that the probability of at least 10 mm of rain in the subsequent week is more than 0.7

(Virmani [24]). Similarly, the date of withdrawal of monsoon is defined as the date up to which a rainfall of at least 30 mm has been received in a week with no subsequent rainfall for at least 3 consecutive weeks towards the end the monsoon season (Shanker et al. [21]).

2.2. Empirical mode decomposition method. The empirical mode decomposition (EMD) is recently developed which is specifically designed to analyze the nonlinear and nonstationary properties of a time-series data (Huang et al. [13]; Gloersen and Huang [9]). There is a straightforward assumption for EMD; all the data must consist of simple intrinsic mode of oscillations. The modes, defined by the EMD method called intrinsic mode functions (IMFs). Figure 2.1 showed the flowchart of IMF computation. EMD naturally separates nonlinear oscillatory patterns of higher frequencies from those of lower frequencies and trend. EMD is very efficient for time-series data (Coughlin and Tung [5]). EMD method separates time-series into intrinsic oscillations using local temporal and structural characteristics of the data. This analysis allows describing the statistical confidence of the study results. The time-series rainfall data is decomposed into locally orthogonal modes using the EMD method (Huang et al. [13]).

There exist many algorithmic approaches of EMD (Flandrin et al. [7]; Ivan and Richard [16]). Time-series data $x(t)$ can be decomposed by EMD as follows:

(1) identify the extrema (both maxima and minima) of data $x(t)$;
(2) generate the upper and lower envelopes $h(t)$ and $l(t)$, respectively, by connecting the maxima and minima points separately with cubic spline interpolation;
(3) determine the local mean $m_1(t) = (h(t) + l(t))/2$;
(4) IMF should have zero local mean, subtract out m_1 from $x(t)$

$$g_1(t) = x(t) - m_1(t); \tag{2.1}$$

(5) test whether $g_1(t)$ is an IMF or not;
(6) repeat steps 1 to 5 and end up with an IMF $g_1(t)$.

Once the first IMF is derived, define $C_1(t) = g_1(t)$, this is the finest temporal scale in the time-series data, that is, the shortest period component of the data $x(t)$. To find all the IMFs, generate the residue $r_1(t)$ of the data by subtracting out $C_1(t)$ from the data as

$$r_1(t) = x(t) - C_1(t). \tag{2.2}$$

The residue now contains information about the components for longer period; it is treated as the new data and is resifted to find additional components.

The sifting process will be continued until it meets a stopping criterion as in Flandrin et al. [7] yielding the subsequent IMFs as well as residues and the result is

$$r_1(t) - C_2(t) = r_2(t), \qquad r_2(t) - C_3(t) = r_3(t), \ldots, \qquad r_{n-1}(t) - C_n(t) = r_n(t), \tag{2.3}$$

where $r_n(t)$ becomes a constant, a monotonic function, or a function with only maxima and one minima from which no more IMF can be derived, Huang et al. [14]. At the end

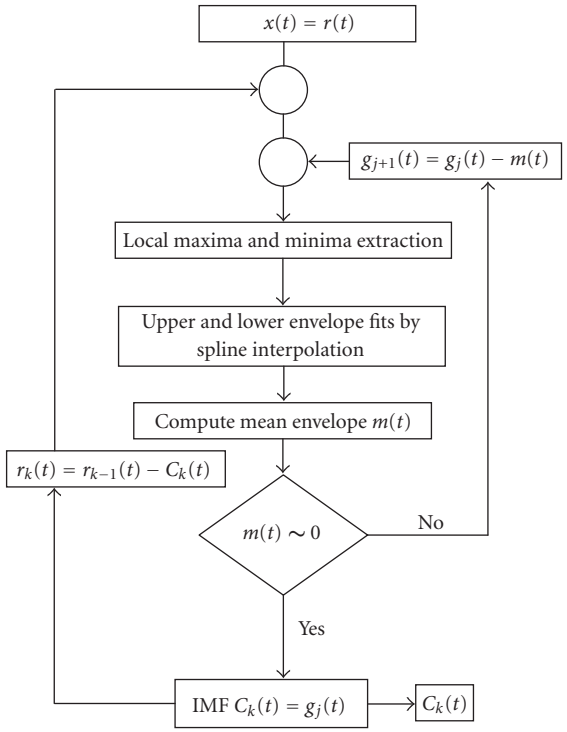

Figure 2.1. Sifting scheme in the empirical mode decomposition.

of the decomposition the signal $x(t)$ is represented as

$$x(t) = \sum_{i=1}^{n} C_i(t) + r_n(t), \tag{2.4}$$

where n is the number of IMFs and $r_n(t)$ is the final residue. Within the entire decomposition, it takes maximum of 810 iterations to generate an IMF.

The IMFs are interpreted as the basis vectors representing the data (Wu and Huang [25]). The EMD can also be treated as dyadic filter bank (Flandrin et al. [7]; Wu and Huang [25]). Each IMF is considered as a bandpass filter (Flandrin et al. [7]); the mean period of any IMF component almost exactly doubles that of the previous one, the Fourier spectra of the IMF components are identical in shape as well as cover the same area on a semilogarithmic period scale (Wu and Huang [25]). It can effectively be applied to the data without harmonics, whereas any harmonic analysis (Fourier, wavelet and so on) would end up in the same context with a much less compact and physically less meaningful decomposition (Chang et al. [2]). The focus in this study will be mainly on the most recent climate records. The data analysis is performed by self-written Matlab programs.

3. Results of EMD analysis and discussion

The data of this investigation has no certainty to contain the harmonic components and EMD is the best-suited method to analyze. The 15-year daily rainfall data and the decomposed intrinsic mode functions (IMFs) are shown in Figure 3.1. The EMD method is very effective on a climate data, the IMFs components are normally distributed and also the energy density of IMF is χ^2-distribution. This result is consistent with the findings of Wu and Huang [25]. The results are statistically significant of information content for IMF components.

3.1. Instantaneous frequency. The instantaneous frequency (IF) represents the signal's frequency at every time instance. IF is defined as the rate of change of the phase angle at the analysis time instant of the analytic version of the signal. Every IMF is a real valued signal and analytic signal method (Cooke [4]) is used to calculate the instantaneous frequency of the IMFs.

The analytic (complex) signal corresponding to a real signal ith IMF $C_i(t)$ is defined as

$$z_i(t) = C_i(t) + jH\left[C_i(t)\right] = a_i(t)e^{j\theta_i(t)}, \tag{3.1}$$

where $H[\cdot]$ is the Hilbert transform operator, $a_i(t)$ and $\theta_i(t)$ are instantaneous amplitude and phase, respectively, of the ith IMF. The Hilbert transform provides a phase shift of $\pm\pi/2$ to all frequency components, whilst leaving the magnitudes unchanged (Cooke [4]). For any arbitrary time-series $X(t)$, the Hilbert transform $Y(t)$ is defined as

$$Y(t) = \frac{1}{\pi} P \int \frac{X(t')}{t - t'} dt', \tag{3.2}$$

where P indicates the Cauchy principal value. With the definition, $X(t)$ and $Y(t)$ form a complex conjugate yielding the analytic signal $Z(t) = X(t) + jY(t)$. The analytic signal is advantageous in determining the instantaneous quantities such as energy, phase, and frequency. So the corresponding instantaneous frequency of the ith IMF can easily be derived as

$$\omega_i(t) = \frac{d\theta_i(t)}{dt}. \tag{3.3}$$

Using (3.1) and (3.3), the analytic signal associated with each of the IMFs and thus the instantaneous frequency of each of them is calculated. The overall effect of IF of all IMFs can be efficiently used as the time-frequency representation of the time domain signal.

3.2. Hilbert spectrum. Hilbert spectrum describes the joint distribution of the amplitude and frequency content of the signal as a function of time. After performing the

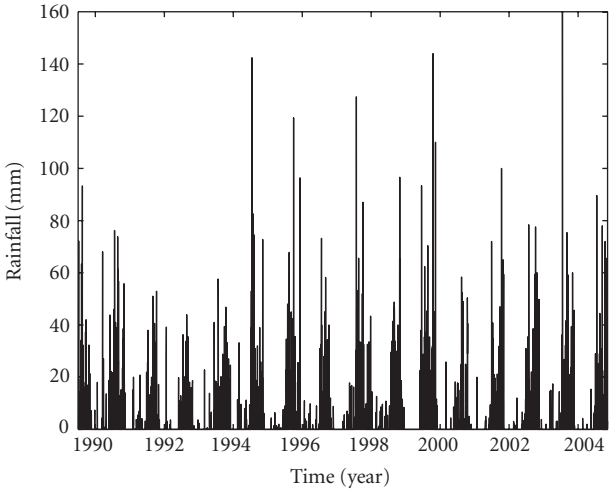

(a)

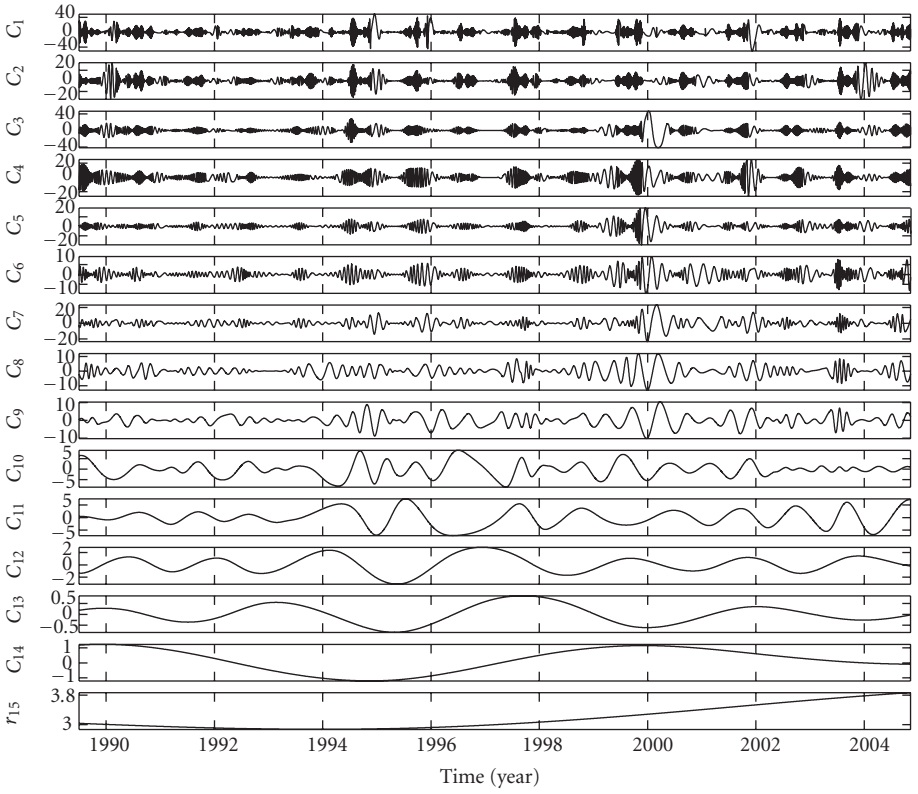

(b)

Figure 3.1. EMD of rainfall data, (a) 15-year daily rainfall (mm), (b) decomposed fourteen IMF components and the final residue.

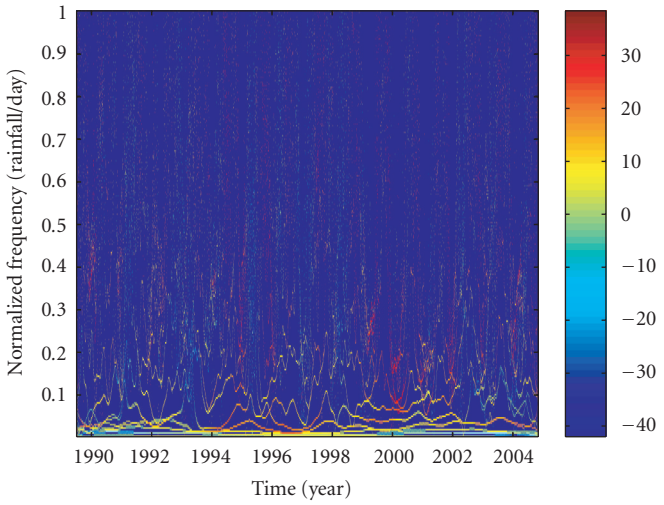

Figure 3.2. Hilbert amplitude spectrum (or simply Hilbert spectrum) of the decomposed rainfall data using 256 frequency bins. The amplitude is in dB.

Hilbert transform on each IMF component, the data can be expressed as

$$x(t) = \sum_{i=1}^{n} a_i(t) e^{j \int \omega_i(t) dt}, \tag{3.4}$$

where only the n IMFs are taken into consideration leaving the residue (Huang et al. [13]). This expression enables to represent the amplitude and instantaneous frequency as a function of time in a three-dimensional plot. This frequency-time distribution of amplitude is designated as Hilbert amplitude spectrum $H(\omega, t)$ or simply Hilbert spectrum.

To build $H(\omega, t)$, the instantaneous frequency of each IMF is first scaled according to the given number of frequency bins. Figure 3.2 represents the Hilbert spectrum (HS) of the rainfall data as shown in Figure 3.1 using 256 frequency bins.

The HS can visualize the data in time and frequency scales at the same time. Regarding the rainfall data, HS makes clear analysis about the distribution and amount of frequent and nonfrequent rainfall at any time over the entire data length. This type of analysis is very much influential in the study of global warming.

There are various forms to present the Hilbert spectrum, the popular form is the color map presentation as shown in Figure 3.2. Any point in the color map presentation corresponds to the energy in dB (determined by the color bar placed at the right side of the HS) at any specific time and frequency.

In this study, the visualization is more preferable than the further processing of the Hilbert spectrum. The smoothened version of the original HS of Figure 3.2 with 3×3 Gaussian filter is shown in Figure 3.3. It appears with more visualization ability of data characteristics in the time-frequency domain than the original one. To improve appearance capability of visual information, the entire time series is divided into two halves and its corresponding HSs are shown in Figure 3.4. Now the data characteristic in the

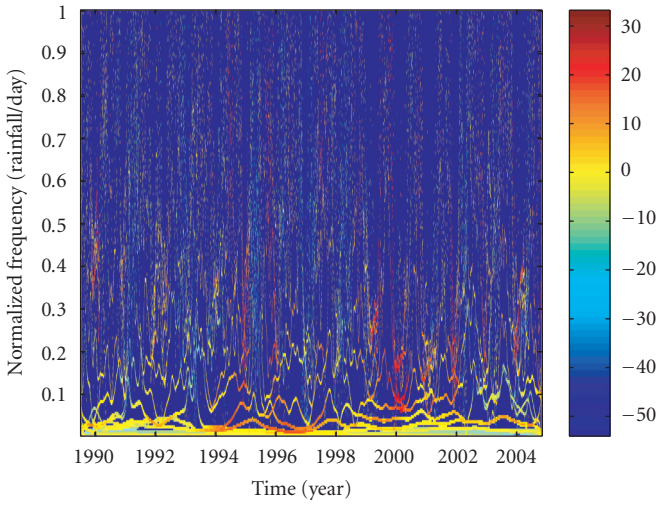

Figure 3.3. Hilbert spectrum of the decomposed rainfall data using 256 frequency bins after 3×3 Gaussian filtering. The amplitude is in dB.

time-frequency domain becomes more understandable than any one of the previous representations.

3.3. Marginal Hilbert spectra. The marginal spectrum defines a measure of total energy contribution from each frequency value. It represents the cumulated amplitude over the entire data length in a probabilistic sense. As we have already derived the Hilbert spectrum $H(\omega, t)$, the marginal spectrum $h(\omega)$ can be easily defined as

$$h(\omega) = \int_t H(\omega, t)dt. \tag{3.5}$$

Figure 3.5 shows the marginal Hilbert spectrum (solid line) as well as the Fourier spectrum (dotted line). These two spectra actually offer different meaning. In Fourier spectrum, the existence of energy at any frequency ω means a component of a sine or a cosine wave persisted through the time span of the data.

However, in marginal Hilbert spectrum, the energy at the frequency ω means there is a higher likelihood that an oscillation with such a frequency exists. Comparing the two spectra in Figure 3.5, the Fourier spectrum is merely representing the nature of harmonic analysis without considering the existence of harmonics in the data; whereas, the marginal Hilbert spectrum appears as nonharmonic, data adaptive spectral distribution. It is also representing the real nature of data, for example, the marginal energy is decreasing with the increase of frequency as visualized in Hilbert spectrum. Since there is a less guarantee of having harmonics in the fully discrete rainfall data, EMD is more suited in analysis than using any other harmonic analysis method (e.g., Fourier, wavelet, and so on).

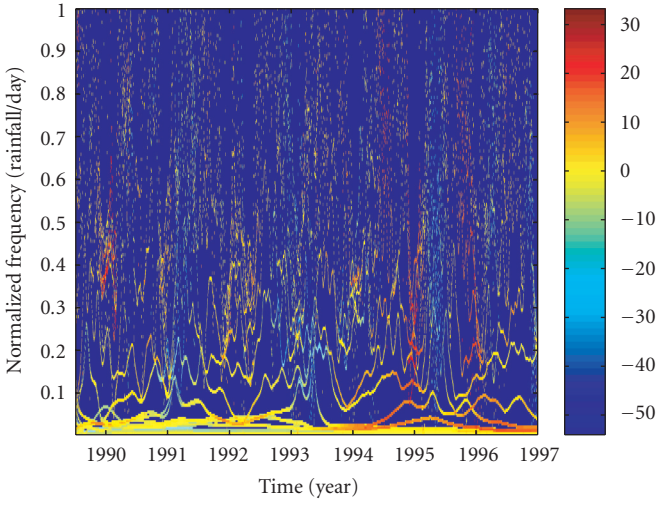

(a)

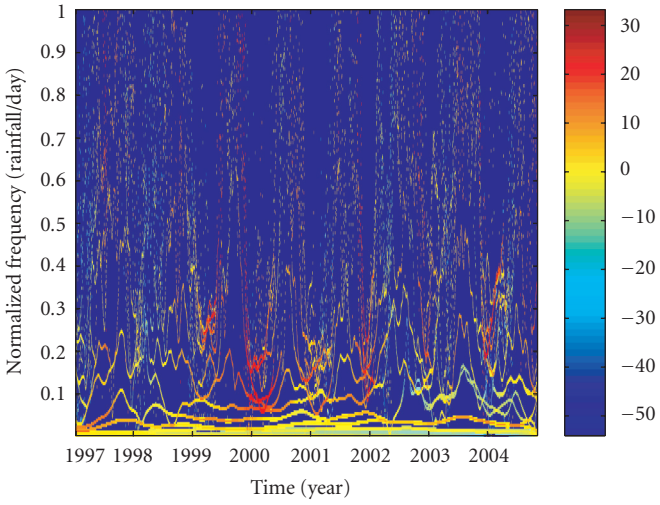

(b)

Figure 3.4. (a) Hilbert spectrum with 3×3 Gaussian filtering of a part of the rainfall data (1989 to 1997 for better visualization) using 256 frequency bins. The amplitude is in dB. (b) Hilbert spectrum with 3×3 Gaussian filtering of a part of the rainfall data (1997 to 2004 for better visualization) using 256 frequency bins. The amplitude is in dB.

3.4. Probability distribution function of the IMF components. The study which examines the probability distribution of an individual IMF (C1 to C14) is shown in Figure 3.6. The probability density function for each IMF is approximately normally distributed, which is evident from the superimposed fitted normal distribution function. From the large sample theory, this fit is expected from central limit theorem.

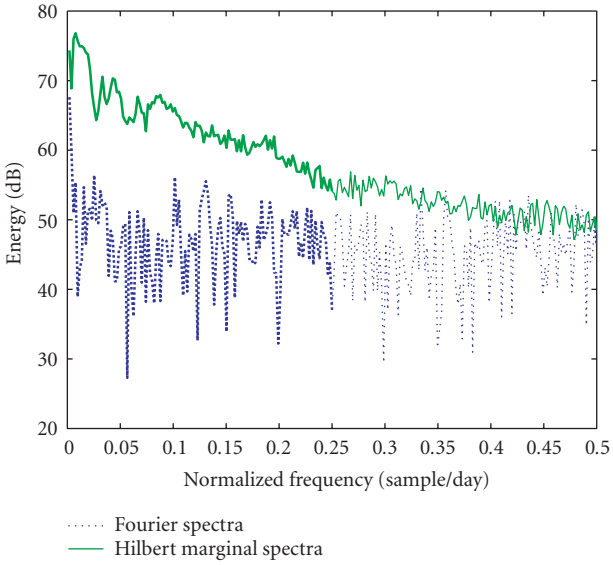

Figure 3.5. Comparison of marginal Hilbert spectrum with Fourier spectrum.

Definitely the deviation from the normal distribution function grows as the mode number increases, Figure 3.6. This is because, in the higher-frequency modes, the IMFs contain a smaller number of oscillations; therefore, the number of events decreases and the distribution becomes less smooth. When sample size is large, the IMFs of the higher-frequency modes will have more oscillations and the distribution will follow the normal distribution according to the central limit theorem. The energy of the probability density function theory for a time series that has a normal distribution should have a χ^2-distribution (Papoulies [17]). IMFs isolate physical processes of various time scales and also give the temporal variation with the processes in their entirety without resorting to the linear assumptions. The IMFs can show the nonlinear distortion of the waveform locally as discussed by Huang et al. [13] and Wu et al. [26]. Finally, IMFs can be effectively used to construct the time-frequency distribution in the form of a Hilbert spectrum, which offers details of the time variation of the underlying processes.

3.5. Completeness and orthogonality of the decomposition. A new technique for analyzing the special scaling structure of rainfall fields has been discussed. An EMD analysis in linearly decomposes the spatially distributed rainfall data into a set of intrinsic mode functions, which are approximate by mutually orthogonal and sum back to the original data.

The sum of all the IMF components reconstructs the original data as shown in Figure 3.7. Considering the entire data length, the maximum difference between the original and reconstructed data is of the order 10^{-14} as shown in Figure 3.7. Now it becomes clear

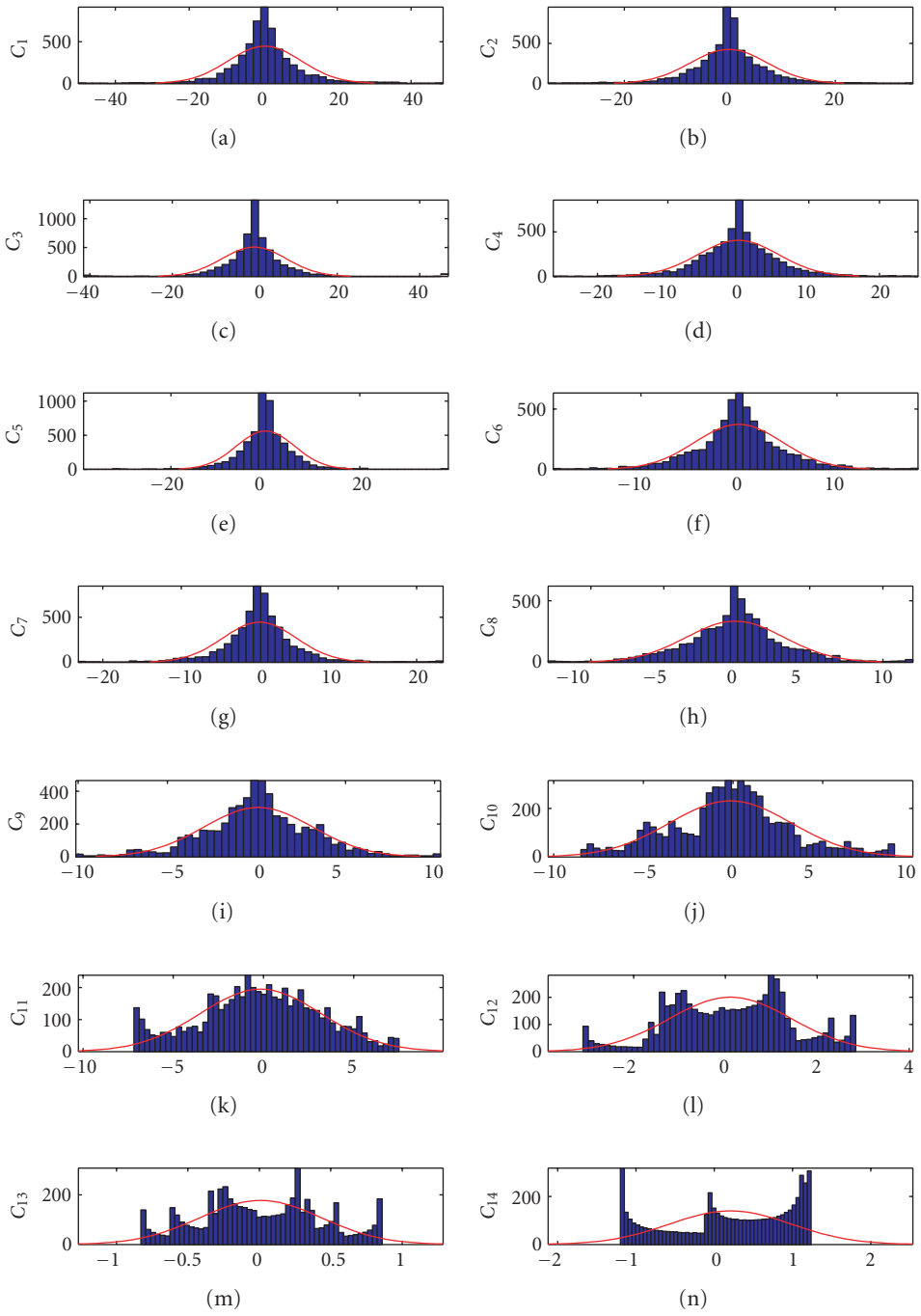

Figure 3.6. Probability distribution functions of the IMF components.

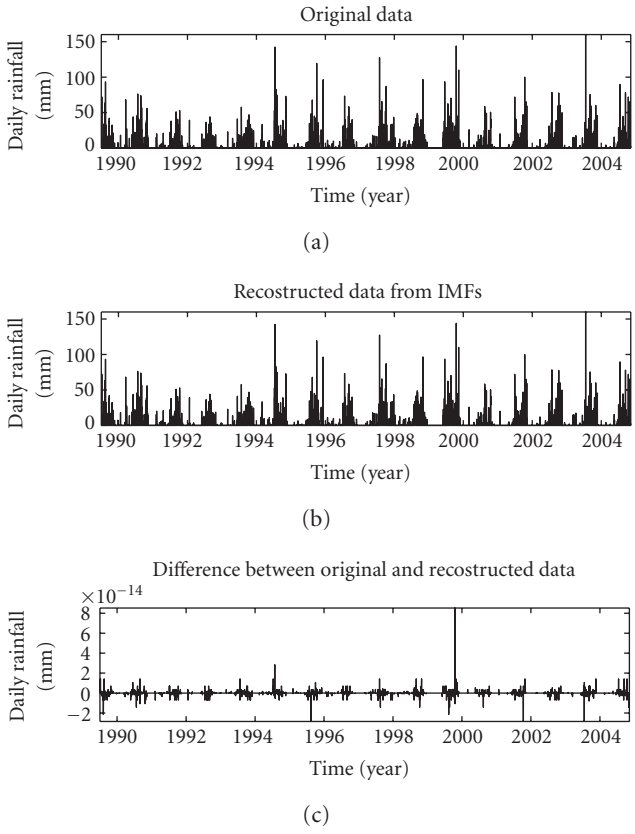

Figure 3.7. The reconstructed rainfall data and the error with the original data.

that EMD is a lossless decomposition and the completeness of the decomposition is thus demonstrated.

To measure the efficiency of the decomposition the orthogonality of the decomposition should also be checked. The elements should be locally orthogonal to each other. The higher orthogonality corresponds to less amount of information leakage (cross terms of the data between the components) between the elements. The amount of leakage usually depends on the length of data as well as the decomposition method (Huang et al. [13]). To check the orthogonality of IMFs from the EMD, an overall index of orthogonality, IO, is defined (Chang et al. [2]) as

$$\mathrm{IO} = \frac{1}{T}\sum_{t}\frac{1}{x^2(t)}\left(\sum_{l}^{n+1}\sum_{m}^{n+1} C_l(t)\cdot C_m(t)\right), \tag{3.6}$$

where l and m stand for the indices of IMFs. The residue is also included to evaluate the IO and that is why l and m are extended to $n+1$ instead of n. In the decomposition of the above-described rainfall data the overall IO value is only 0.00025.

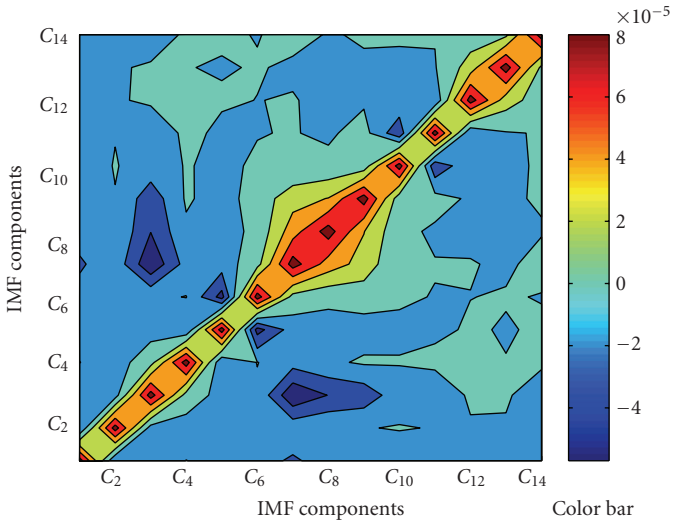

Figure 3.8. The values of the indices of orthogonality between all possible pairs of IMFs.

The orthogonality can also be measured for any pair of components C_l and C_m as

$$\mathrm{IO}_{l,m} = \frac{1}{T}\sum_{t}\frac{C_l(t)\cdot C_m(t)}{C_l^2(t)+C_m^2(t)}. \tag{3.7}$$

A set of perfect orthogonal IMF components will give zero values of IO and $\mathrm{IO}_{l,m}$. In practice, the accepted solution for those with IO and $\mathrm{IO}_{l,m}$ are smaller than 0.100.

The orthogonality values between all possible pairs of IMF components are shown as the contour map in Figure 3.8. The color value (indicated by the color bar) in the contour map represents the index on orthogonality between the corresponding pair (obtained from x- and y-axes) of IMF components. It is noted that the maximum value of the indices of orthogonality is of the order 8×10^{-5} which is very much less than the proposed value of 0.100. By observing the completeness and orthogonality, the study concluded that the EMD method is well fitted to analyze the mentioned rainfall data.

3.6. Degree of stationarity test. EMD as well as Hilbert spectrum is more suitable for nonstationary data. If $h(\omega)$ is the marginal Hilbert spectrum, the mean marginal spectrum $\mu(\omega) = (1/T)h(\omega)$. Then the degree of stationarity (DS) is defined as

$$D_s(\omega) = \frac{1}{T}\int_t \left(1 - \frac{H(\omega,t)}{\mu(\omega)}\right)^2 dt. \tag{3.8}$$

It gives the measure of the degree of stationarity at any frequency over the entire data set and it produces the zero value for a stationary process or data set. With a stationary data set, the Hilbert spectrum is not a function of time; it will consist of only horizontal contour lines. The DS of the rainfall data is shown in Figure 3.9 with 256 frequency bins

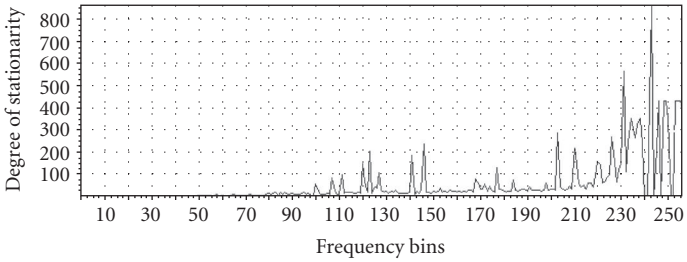

Figure 3.9. Degree of stationarity of the rainfall data (with 256 frequency bins).

Table 3.1. Some valuable parameters of IMF components.

IMF	Mean period	% of energy	% of variance	No. of iteration
C1	0.1659	14.4535	26.4186	810
C2	0.1211	10.7613	14.3364	789
C3	0.0888	10.6405	16.4239	796
C4	0.0658	9.0848	10.2414	682
C5	0.0501	8.8845	8.8665	553
C6	0.0364	7.1759	5.3736	229
C7	0.0243	7.0227	5.9021	31
C8	0.0146	5.4684	3.0393	82
C9	0.0091	5.1021	2.4954	14
C10	0.0045	5.8461	3.1122	15
C11	0.0023	6.1588	3.0762	13
C12	0.0012	2.4761	0.4754	6
C13	0.0007	0.8026	0.0491	5
C14	0.0004	1.5317	0.1634	6

(same as the number used in Hilbert spectrum). As the index showed, the data are highly nonstationary especially for the high-frequency components. Also from the scenario by observing the Hilbert spectrum, there exists more regularity in the data at the lower frequency range and less in the higher-frequency bins. This provides a qualitative measure of the degree of stationary. The quantitative measure of DS ensures that the rainfall data is nonstationary and EMD is more suited for analyzing the data.

3.7. Parameters of IMF components and its properties. Some other properties of the IMF components can also be useful to understand easily the analysis method of 15-year rainfall data. The parameters values computed from the rainfall data are listed in Table 3.1. The mean period (calculated as the total number of extrema divided by the number of data samples) serves the information that how the EMD works as the filter bank in

data analysis. The percentage of energy content represents how much energy of the data is contained by each IMF components and the variance offers the amount of information by corresponding IMF. Finally the number of iteration required to compute individual IMF provides the idea about the computational cost of the analysis. The empirical findings are almost identical to those reported by Flandrin et al. [7].

4. Conclusions

This study plays a vital role for analyzing the properties of nonlinear and nonstationary daily rainfall time-series data. This study focuses on the relation between the rainfall variability and global warming using EMD data analyzing method. The results showed that most of the IMFs have normal distribution. Therefore, the energy density distribution of an IMF samples satisfies χ^2-distribution. An EMD analysis linearly decomposes the spatially distributed rainfall data into a set of intrinsic mode functions, which are approximate by mutually orthogonal and sum back to the original data. The EMD analysis successively extracts the IMFs starting with the highest local spatial frequencies in a recursive way, which is effectively a set of successive low-pass spatial filters based entirely on the properties exhibited by the data. The IMFs are more effective in isolating physical processes of various time scales and also statistically significant. The major peak of frequencies also appears to be located around the peaks of the decadal variability. The results of this study indicate that this may be the response to decadal climate variability and global warming. The EMD is a new approach to many researchers in climate research. This study suggests that the recent global warming along with decadal climate variability contributes not only to the more extreme warm events, but also to more frequent, long lasting drought and flood.

References

[1] R. Balocchi, D. Menicucci, E. Santarcangelo, L. Sebastiani, A. Gemignani, B. Gellarducci, and M. Varanini, *Deriving the respiratory sinus arrhythmia from the heartbeat time series using empirical mode decomposition*, Chaos, Solitons and Fractals **20** (2004), no. 1, 171–177.

[2] C. Y. Chang, N. E. Huang, and Z. Shen, *A statistically significance periodicity in the homestake solar neutrino data*, Chinese Journal of Physics **35** (1997), no. 6–11, 818–831.

[3] F. Chiew, M. Peel, G. Amirthanathan, and G. G. S. Pegram, *Identification of oscillations in historical global streamflow data using Empirical Decomposition*, Seventh IAHS Scientific Assembly-Symposium on Regional Hydrological Impacts of Climate Variability and Change with an Emphasis on Less Developed Countries, 2004.

[4] M. Cooke, *Modeling Auditory Processing and Organisation*, Cambridge University press, Cambridge, 1993.

[5] K. Coughlin and K. K. Tung, *Eleven year solar cycle signal throughout the lower atmosphere*, Journal of Geophysical Research **109** (2004), D21105.

[6] A. V. Fedorov and S. G. Philander, *Is El Niño changing?*, Science **288** (2000), no. 5473, 1997–2002.

[7] P. Flandrin, G. Rilling, and P. Goncalves, *Empirical mode decomposition as a filter bank*, IEEE Signal Processing Letters **11** (2004), no. 2, 112–114.

[8] M. H. Glantz, R. W. Katz, and N. Nicholls (eds.), *Teleconnections Linking Worldwide Climate Anomalies*, Cambridge University Press, Cambridge, 1991.

[9] P. Gloerson and N. E. Huang, *Comparison of interanual intrinsic modes in hemispheric sea ice covers and others geophysical parameters*, IEEE Transactions on Geoscience and Remote Sensing **41** (2003), no. 5, 1062–1074.

[10] D. Harris, E. Foufoula-Georgiou, K. K. Droegemeier, and J. J. Levit, *Multiscale statistical properties of a high-resolution precipitation forecast*, Journal of Hydrology **2** (2001), 406–418.

[11] D. E. Harrison and N. K. Larkin, *Darwin sea level pressure, 1876-1996: evidence for climate change?*, Geophysical Research Letters **24** (1997), no. 14, 1779–1782.

[12] N. E. Huang, Z. Shen, and S. R. Long, *A new view of non-linear water waves: the Hilbert spectrum*, Annual Review of Fluid Mechanics, Vol. 31, Annu. Rev. Fluid Mech., vol. 31, Annual Reviews, California, 1999, pp. 417–457.

[13] N. E. Huang, Z. Shen, S. R. Long, M. C. Wu, H. H. Shih, Q. Zheng, N.-C. Yen, C. C. Tung, and H. H. Liu, *The empirical mode decomposition and the Hilbert spectrum for nonlinear and non-stationary time series analysis*, Proceeding of the Royal Society of London. Series A. **454** (1998), 903–995.

[14] N. E. Huang, M.-L. Wu, W. Qu, S. R. Long, and S. S. P. Shen, *Application of Hilbert-Huang transform to non-stationary financial time series analysis*, Applied Stochastic Modelels in Business and Industry **19** (2003), no. 3, 245–268.

[15] P. A. Hwang, N. E. Huang, and D. W. Wang, *A note on analyzing nonlinear and nonstationary ocean wave data*, Applied Ocean Research **25** (1999), no. 4, 187–193.

[16] M. C. Ivan and G. B. Richard, *Empirical mode decomposition based frequency attributes*, Proceedings of the 69th SEG Meeting, Texas, 1999.

[17] A. Papoulies, *Probability, Random Variable and Stochastic Processes*, 2nd ed., McGraw-Hill, New York, 1986.

[18] G. G. S. Pegram and A. N. Clothier, *High resolution space—time modelling of rainfall: the "String of Beads" model*, Journal of Hydrology **241** (2001), no. 1-2, 26–41.

[19] B. Rajagopalan, U. Lall, and M. A. Cane, *Anomalous ENSO occurrences: an alternative view*, Journal of Climate **10** (1997), no. 9, 2351–2357.

[20] ———, *Comment on reply to the comments of Trenberth and Hurrell*, Bulletin of American Meteorological Society **80** (1999), 2724–2726.

[21] U. Shanker, K. K. Agrawal, and V. K. Gupta, *Rainfall pattern and strategy for Jabalpur region*, Indian Journal of Agricultural Sciences **62** (1992), no. 1, 58–59.

[22] S. Sinclair and G. G. S. Pegram, *Empirical Mode Decomposition in 2-D space and time: a tool for space-time rainfall analysis and nowcasting*, Hydrological Earth System Sciences Discussions **2** (2005), 289–318.

[23] B. J. Turner, I. Zawadzki, and U. Germann, *Predictability of precipitation from continental radar images. Part III: operational nowcasting implementation (MAPLE)*, Journal of Applied Meteorology **43** (2004), 231–248.

[24] S. M. Virmani, *Agricultural climate of hyderabad region—a analysis for semi-arid tropics*, Tech. Rep., 1975, 13–24.

[25] Z. Wu and N. E. Huang, *A study of the characteristics of white noise using the empirical mode decomposition method*, Proceedings of the Royal Society of London. Series A **460** (2004), no. 2046, 1597–1611.

[26] Z. Wu, E. K. Schneider, Z. Z. Hu, and L. Cao, *The impact of global warming on ENSO variability in climate records*, Tech. Rep. CTR 110, COLA, Maryland, 2001.

[27] C. Wunsch, *The interpretation of short climate records, with comments on the North atlantic and Southern Oscillations*, Bulletin of the American Meteorological Society **80** (1999), no. 2, 245–255.

[28] R. R. Zhang, S. Ma, and S. Hartzell, *Signatures of the seismic source in EMD-based characterization of the 1994 Northbridge, California, earthquake recording*, Bulletin of the Seismological Society of America **93** (2003), no. 1, 501–518.

Md. Khademul Islam Molla: Department of Frontier Informatics, The University of Tokyo, 7-3-1 Hongo, Bunkyo-ku, Tokyo 113-0033, Japan
E-mail address: molla@gavo.t.u-tokyo.ac.jp

M. Sayedur Rahman: Center for Climate System Research, The University of Tokyo, 5-1-5 Kashiwanoha, Kashiwa-shi, Chiba 277-8568, Japan
E-mail address: rahman@ccsr.u-tokyo.ac.jp

Akimasa Sumi: Center for Climate System Research, The University of Tokyo, 5-1-5 Kashiwanoha, Kashiwa-shi, Chiba 277-8568, Japan
E-mail address: sumi@ccsr.u-tokyo.ac.jp

Pabitra Banik: Agricultural Science Unit, Indian Statistical Institute, Kolkata, India
E-mail address: pbanik@isical.ac.in